High-dimensional neural network potential for liquid electrolyte simulations

Steven Dajnowicz[1‡*], Garvit Agarwal[1‡*], James M. Stevenson[1], Leif D. Jacobson[2], Farhad Ramezanghorbani[1], Karl Leswing[1], Richard A. Friesner[1,3], Mathew D. Halls[4], Robert Abel[1]

1) Schrödinger, Inc., New York, New York 10036, United States

2) Schrödinger, Inc., Portland, Oregon 97204, United States

3) Department of Chemistry, Columbia University, New York, New York 10027 United States

4) Schrödinger, Inc., San Diego, California 92121, United States

ABSTRACT: Liquid electrolytes are one of the most important components of Li-ion batteries, which are a critical technology of the modern world. However, we still lack the computational tools required to accurately calculate key properties of these materials (viscosity, ionic diffusivity) from first principles necessary to support improved designs. In this work, we report a machine learning-based force field for liquid electrolyte simulations which bridges the gap between the accuracy of range-separated hybrid density functional theory and the efficiency of classical force fields. Predictions of material properties made with this force field are quantitatively accurate compared to experimental data. Our model uses the QRNN deep neural network architecture, which includes both long-range interactions and global charge equilibration. The training dataset is composed solely of non-periodic DFT, allowing the practical use of an accurate theory (here, ωB97X-D3BJ/def2-TZVPD) which would be prohibitively expensive for generating large datasets with periodic DFT. In this report we focus on seven common carbonates and $LiPF_6$, but this methodology has very few assumptions and can be readily applied to any liquid electrolyte system. This provides a promising path forward for large scale atomistic modeling of many important battery chemistries.

INTRODUCTION

The development of rechargeable Li-ion batteries (LIBs) has revolutionized electric vehicles and portable electronic devices[1, 2]. Yet, further advancements are needed to improve the power, safety, reliability, and lifetime of LIBs—such advances are required to enable grid-level energy storage and the operation of electric vehicles for commercial applications[3, 4]. Over the past few decades, atomistic modeling of battery materials has complemented experimental characterization techniques and become an important part of the development of new technologies[5-7]. Widespread application of computational methods is contingent on their ability to quantitatively predict key properties that drive material design. In addition, for such methods to be truly predictive they should be free of parameters based on experimental data, which for prospective exploration of materials may not exist. For LIBs, some of the key properties are ionic mobility, viscosity of liquid electrolytes, thermal and electrochemical stability of electrolytes, and equilibrium voltage.

Despite its high computational cost, ab initio molecular dynamics (AIMD) density functional theory[8, 9] (DFT) is the workhorse method for modeling battery materials at the atomic and electronic scales. For many systems it is the only method with sufficient accuracy while still being computationally tractable, and even then only for short time and length scales[5, 7]. For example, AIMD simulations have provided valuable insights into the decomposition pathways of ethylene carbonate (EC) on the surface of graphite electrodes[10-12]. In addition, DFT studies have contributed to the understanding of decomposition reactions of other common carbonates and the exfoliation process of graphite due to co-intercalation of propylene carbonate[13-17]. However, simulations are typically restricted to a few hundred atoms and picosecond time scales. Reliable predictions of dynamic bulk properties of liquids, such as viscosity and diffusivity require longer time scales than are typically infeasible with AIMD. One of the least understood components—but essential for stable operation—of LIBs is the solid electrolyte interphase (SEI), which is a mosaic structure that is formed on the electrode surfaces from the products of electrolyte decomposition[18]. The

formation of SEI involves a series of complex chemical reactions that are not well understood and spans several length and time scales, making it difficult to probe both experimentally and computationally. Therefore, alternative methods that are capable of accurately modeling larger length and time scales must be considered to aid in the development of the next generation of LIBs.

Empirically fitted force fields are complementary methods that allow large-scale atomistic simulations[19]. The use of simple analytic formulas to describe interatomic interactions in these models significantly reduces the computational cost by several orders of magnitude compared to DFT, but at the expense of accuracy. Development of traditional force fields relies on a cumbersome parameterization and validation process. This parameterization process tries to map each atom to a set of parameters that represents the interatomic interactions by fitting the model to experimental and/or quantum chemical data. When parametrized for a specific task, both fixed charge and polarizable force fields have been shown to accurately model structural, thermodynamic and transport properties of bulk electrolytes and anode electrolyte interfaces[20-22]. Furthermore, the reductive decomposition of ethylene carbonate using eReaxFF[23], a reactive force field, was consistent with DFT simulations[24]. ReaxFF has also been used for modeling the formation and growth of the SEI[25, 26]. Nonetheless, like most other reactive force fields, eReaxFF and ReaxFF suffers from a lack of transferability and must be reparametrized for each system of interest.

A promising alternative is machine learning-based force fields (MLFFs)[27]. Unlike traditional force fields, these make few prior assumptions about the shape of the interatomic potentials. These models are more computationally efficient than quantum chemical methods and can achieve chemical accuracy relative to the method they are trained to reproduce[28-34]. Furthermore, MLFFs have shown to accurately reproduce both equilibrium and reactive regions of the PES[27], while traditional empirically fitted force fields have trouble with reactive systems without major modifications to the functional form and substantial parameterization. In essence, MLFFs are constructed by applying a regression algorithm to a highly flexible functional form such as Gaussian process regression, and kernel rigid regression, or high-dimensional neural network potentials (HDNNPs). A key step that affects the performance of MLFFs is the

featurization, which transforms the input (atomic coordinates and net charge) into "model readable" data that enforces symmetry and locality. For comprehensive reviews on MLFFs, see the article by Behler[27] and the article by Deringer et al[35].

In the context of battery materials research, MLFFs are starting to be developed to address the practical problems discussed above[35-37]. The greatest focus has been on various chemistries related to anode materials. Specifically, new models have been developed to study bulk anode phases[38], and intercalation of alkali-metals in disordered carbon anodes materials[39]. Some progress has also been made modeling Li^+ diffusion in a solid electrolyte material[40]. However, to date, application of machine learning models to liquid electrolytes and electrode/electrolyte interfaces are limited[35-37], which we view as the most relevant systems from a practical perspective.

In this report, we construct a HDNNP, utilizing the recently reported charge recursive neural network architecture (QRNN)[28], for liquid electrolyte simulations. The model was trained using an active learning approach[41-44] . In addition, the QRNN was trained exclusively to non-periodic DFT cluster data without any parametrization against experimental data (Scheme 1), a strategy that has been proven to be successful for liquid water[45]. With the addition of $LiPF_6$, the common carbonates that we selected for this study were EC, propylene carbonate (PC), vinylene carbonate (VC), fluoroethylene carbonate (FEC), dimethyl carbonate (DMC), diethyl carbonate (DEC), and ethyl methyl carbonate (EMC). The chemical structures of all the 7 carbonate solvents and the PF_6^- anion are depicted in Figure S1 of the SI. These seven carbonates were selected based upon their widespread use in LIBs and the availability of experimental values of liquid thermodynamic and transport properties for comparison with the predicted values. In this work, we focus on the comparison between the predicted values from our QRNN model to experimental bulk thermodynamic and transport properties of pure carbonate solvents and electrolyte mixtures over a range of temperatures and salt concentrations. Overall, the predicted bulk properties from the QRNN electrolyte model agrees well with experimental observations. This lays the foundation to extend

our model generalizability to accurately predict more complicated chemistries that occur during reactions at the electrode/electrolyte interface.

RESULTS AND DISCUSSION

QRNN performance on cluster test set: We trained a QRNN[28] force field to a relatively small (~360K data points compared to ~5M for ANI-1x[46]) dataset of electrolyte clusters, including common carbonate solvents (EC, PC, VC, FEC, DMC, DEC, EMC), Li^+, and PF_6^- ions. To evaluate the model performance, we constructed an independently sampled test set of 2.5k cluster data points extracted from the production NPT trajectories of pure carbonate solvents and electrolyte mixtures. For the cluster extraction details please refer to the subsection Dataset Construction in the Methods section. This test set includes clusters from dimers to heptamers, thus containing cluster sizes that are not in the training dataset, which stops at hexamers. Here we compare the absolute energies (Figure 1a), dipoles components (Figure 1b), and force components (Figure 1c) relative to the reference level of theory (ωB97X-D3BJ/def2-TZVPD). The energy, dipole, force RMSEs are 0.40 kcal mol^{-1}, 0.11 Debye, and 0.47 kcal mol^{-1} $Å^{-1}$, respectively. Overall, the QRNN electrolyte model shows good performance on the cluster test set, which is necessary but not sufficient for accuracy in the liquid state since the model was trained on cluster data. Therefore, the more stringent and useful tests for our model are quantitatively accurate predictions of thermodynamic and transport properties of liquid electrolytes compared to experiments. These tests are discussed in the following sections.

Thermodynamic and transport properties of liquid carbonate solvents: Prediction of the thermodynamic and transport properties of bulk liquids requires stable simulations over fairly large time and length scales: 1000+ atoms in size and > 500 ps of molecular dynamics (MD). Therefore, the stability of the QRNN electrolyte model was exhaustively tested by running MD simulations of our systems of interest. We analyzed the final state of each system, distributions of bond distances of the molecules during the MD trajectories, and temporal evolution of total energy of the system to ensure that the system did not undergo any spurious chemical reactions or energy drift. Additional details are provided in the SI.

Once we were confident in our ability to run long time-scale MD simulations, we validated the accuracy of the QRNN potential by comparing the bulk thermodynamic properties (density, specific heat at constant volume (C_v) and heat of vaporization (H_{vap})) and transport properties (self-diffusivity and viscosity) computed using the MD simulations to experimental data. The selection of the above properties was motivated by the availability of experimental data in the literature and their relevance for the design of liquid electrolytes for LIBs. All the properties were computed at a temperature of 298 K for all the solvents except for EC and FEC, where the simulations were performed at a temperature of 313 K to match the conditions of available experimental data. We also computed the same properties using the OPLS4 force field[47] as a benchmark of the performance of more traditional methods. A detailed comparison of the computed properties (using QRNN and OPLS4) against the available experimental data is shown in Figure 2 and summarized in Table S2, S3 of the SI.

The QRNN computed density, H_{vap} and C_V for each of the pure solvents are in excellent agreement with the experimental data[21, 48-56] as shown in Figure 2 (a), (b) and (c), respectively. Similarly, the OPLS4 gives good predictions of the density and the heat of vaporization for all the solvents but overestimates the Cv values as compared to experimental data[21, 48-56]. The root-mean-squared error (RMSE) of the QRNN and OPLS4 predicted densities is 0.030 g/cm^3 and 0.029 g/cm^3, respectively suggesting similar performance of both the force fields for density prediction of pure liquid solvents. However, QRNN gives better predictions of H_{vap} with a lower RMSE of 3.23 kJ/mol compared to 9.15 kJ/mol for OPLS4 predictions.

The accurate prediction of viscosities from liquid simulations is more challenging compared to the prediction of bulk thermodynamic properties[57]. Nonetheless, QRNN computed viscosity values are in excellent agreement with the experimentally measured values[54, 56, 58] as shown in Figure 2 (d), apart from the underestimation for DEC. On the other hand, OPLS4 systematically overestimates the experimental viscosities by a significant amount for all the pure carbonate solvents. The lower RMSE of the QRNN computed viscosities (~0.31 cP) as compared to OPLS4 computed values (~1.06 cP) indicates that the

viscosity prediction of the pure solvents can be significantly improved by the QRNN force field. The experimental self-diffusivity data[59] is available for only 3 (EC, PC and DMC) out of the 7 carbonate solvents considered in the paper. In general, both QRNN and OPLS4 force fields underestimate the self-diffusivities compared to the experimental data[59] as shown in Figure 2 (e). However, the QRNN computed self-diffusivity for PC and DMC solvents are in better agreement with the experimental value[59] as compared to the OPLS4 computed value. For pure EC solvent, QRNN and OPLS4 under-predict the diffusivity values by 40% and 25%, respectively. Overall, the QRNN force field affords significant improvement in the predicted properties for the pure solvents as compared to the OPLS4.

Temperature Dependence of Viscosity for EC and PC: To further demonstrate the capabilities of the QRNN force field, we computed the viscosities of liquid EC and PC solvents over a wide temperature range and compared the results against experimental data[60]. For liquid EC, the simulations were performed at temperatures in the range of 313 K to 473 K, and for PC, 298 K to 423 K, to match the available experimental data[60]. The comparison of the QRNN and OPLS4 computed viscosities with the experimental data is shown in Figure 3 (a), (b) and summarized in Table S4 of the SI. The QRNN and OPLS4 computed viscosities for EC are in excellent agreement with the experimental values[60] over the entire temperature range. For liquid PC, OPLS4 overestimates the viscosity values compared to experimental data[60] at lower temperature, whereas the QRNN predicted viscosities are in excellent agreement with experimental values (within 0.2 cP).

Salt Concentration Dependence of Viscosity of Electrolyte Mixtures: For LIB design it is critical to understand the effect of salt concentration on the viscosities of mixed solvent electrolytes. Here, we used a 3: 7 weight % mixture of EC: DMC solvents with varying concentrations (0-2 m (mol/kg)) of $LiPF_6$ salt to match the experimental conditions[61]. Such solvent blends, mixture of EC with lower viscosity linear carbonate solvent, are routinely used as electrolytes for LIBs. The viscosities of the electrolyte mixture are computed using QRNN and OPLS4 force fields at a temperature of 313 K and compared against experimental data[61] as shown in Figure 4. OPLS4 consistently overestimates the viscosity values for all

salt concentrations. The QRNN computed viscosities show excellent agreement with the experimental values[61] up to a salt concentration of 1.0 m. For the high salt concentration electrolytes (> 1 m $LiPF_6$), QRNN significantly overpredicts the viscosity values compared to the experimental data[61] as summarized in Table S5 of the SI.

We have found that the disagreement of the QRNN predicted viscosity values at higher salt concentrations can be attributed to convergence limitations of our current sampling protocol (NVT replicas of 1 ns each) and the small simulation box dimensions (finite size effect) required by our prototype QRNN implementation. We employed the OPLS4 force field (due to its superior computational efficiency) to test the effect of NVT simulation duration (1 ns vs 10 ns) on the convergence of computed viscosity values, as shown in Figure S7 of the SI. The plots demonstrate that 1 ns simulation time is sufficient for the convergence for the low viscosity electrolyte (0 m $LiPF_6$) whereas longer NVT simulation duration of 10 ns is required for the case of high viscosity electrolytes (2 m $LiPF_6$). We also compared the effect of number of atoms (or simulation box size) on the computed viscosity values for the low and high viscosity electrolytes using the OPLS4 force field as shown in Figure S8 of the SI. We observe only a weak dependence of viscosity on the number of atoms for low viscosity electrolytes, which agrees with the results reported in literature[61]. However, for high viscosity electrolyte (i.e., 2 m $LiPF_6$) the computed viscosity increases rapidly as simulation size is below 2000 atoms. Thus, the over-prediction of the viscosity values by the QRNN force field for the high viscosity electrolytes can be attributed to the convergence issues associated with short simulation duration of NVT replicas (i.e., 1 ns) and finite size effects due to small simulation box dimensions (< 1000 atoms) used for current prototype QRNN simulations. More extensive calculations are needed to determine the optimal sampling protocol for high viscosity liquid solutions using the QRNN potential which are beyond the scope of the current work. The simplest approach is to make the QRNN implementation (currently a research prototype in PyTorch[25]) faster and less memory-intensive so that it can handle larger length and time scale simulations.

Temperature Dependence of Diffusivity of Electrolyte Mixtures: Using the QRNN force field, we also computed the self-diffusivity of ions and solvent molecules as a function of temperature for various electrolyte systems. Accurate prediction of the diffusion of ions in the bulk electrolyte is critical for the design of next-generation electrolytes, since higher ion diffusivity values allow faster battery charging and discharging. Here, we computed diffusivities of Li^+, PF_6^- and solvent molecules (EC, PC and DEC) for 3 model electrolytes, i.e., EC + 1M $LiPF_6$, PC + 1M $LiPF_6$ and DEC + 1M $LiPF_6$ for temperature values ranging from 273 K to 353 K. The QRNN predicted diffusivities for the ions and solvents molecules are then compared with the experimental data[62] and the OPLS4 predictions. For the case of DEC + 1M $LiPF_6$, the QRNN computed diffusivities as a function of temperature for the Li^+, PF_6^- ions and DEC solvent molecules agree well with the experimental data as shown in Figure 5. The QRNN computed diffusivities of Li^+ and PF_6^- ions are similar in magnitude whereas the diffusion of DEC solvent molecules is about twice as fast as that of the ions, in good agreement with experimental data. Since QRNN computed diffusivities include a finite size correction for the small simulation boxes, the diffusivity values depend on the computed viscosity values for the electrolyte at each temperature. At higher temperatures of 333 K and 353 K, QRNN over-predicts the diffusivity values for the ions and the DEC solvent molecules which can be correlated to the under-prediction of the viscosity (compared to experimental data) for the pure DEC solvent as discussed earlier. In comparison, OPLS4 consistently under-predicts the computed diffusivities for the ions and the solvent molecules across the entire temperature range of 273 K – 353 K resulting in slower diffusion of the species in the electrolyte. Similar trends are observed for EC + 1M and $LiPF_6$ and PC + 1M $LiPF_6$ as discussed in the SI (Figure S9 and S10). Overall, QRNN accurately reproduces the experimentally measured diffusivity values for the different electrolytes and reproduces the trend of increasing diffusivity of ions and solvent molecules with temperature.

Structural Properties of Electrolytes: To characterize the effect of EC vs DMC on the solvation structure around Li^+ cation, we computed the radial distribution function (RDF) and the average coordination number of the solvent in the first solvation shell of Li^+ ion as shown in Figure 6. The simulations are performed

by equilibrating the electrolyte systems at 298 K and 1 atm pressure for 1 ns using the NPT ensemble. The NPT equilibration is followed by 1 ns NVT simulation at 298 K. The NVT trajectory is utilized to compute the RDF for each electrolyte system. The first solvation shell of Li^+ cation consists of ~3.8 EC and ~3.6 DMC molecules at an average distance of ~3.0 Å for EC + 1M $LiPF_6$, DMC + 1M $LiPF_6$ electrolytes, respectively[20, 63]. The Li-O_c peak positions for the two electrolytes (1.94 Å) are in good agreement with the values reported in the literature[63, 64]. The similar values of RDF peak positions for the EC and DMC electrolytes indicate that the Li-O_c distance is mainly dictated by the electrostatic interactions between the Li^+ cation and the carbonyl oxygen atom of the solvent molecules. This is in good agreement with the trend observed in AIMD simulations in the literature[63]. We analyzed the temporal evolution of the average number of solvent molecules and PF_6^- anions within the first solvation shell of Li^+ cations (within 3 Å) for the EC + 1M $LiPF_6$ and DMC + 1M $LiPF_6$ electrolytes during the 1 ns NVT trajectory to understand the composition of the Li^+ solvation shell during the MD trajectory as discussed in Figure S11 of the SI.

Conclusion: We report the development and validation of a HDNNP for liquid electrolyte simulations, comparing it against its reference level of DFT, against experiment, and against a highly optimized general purpose force field with traditional functional form (OPLS4). Overall, OPLS4 performs reasonably for some properties but it is not reliable for all properties (e.g., C_v, viscosity and diffusivity). It is well-known that QM-based charge fitting can improve the bulk properties of liquid systems when using classical force fields[20, 21, 64]. However, it is not our focus to develop parameterization methods to improve the performance of the OPLS4. In comparison, the QRNN electrolyte potential very accurately predicts thermodynamic and transport properties across a subset of chemical compounds the are utilized in industrial liquid electrolytes. Specifically, the dynamic charge model in the QRNN architecture can describe charge transfer and polarization effects, which are important when modeling ionic systems like electrolytes[28]**.** Overall, our results show promise for building a general liquid electrolyte model.

We accomplished accurate bulk property predictions by training the QRNN electrolyte model against gas-phase molecular clusters without any empirical parameterization. This highlights the accuracy and transferability of the range-separated hybrid ωB97X-D3BJ functional used to generate energy, forces, and dipole labels for our training data. Training to a gas-phase clusters dataset allows higher level DFT reference labels, which are impractical for a periodic dataset. MLFFs that are trained to periodic datasets are typically trained to pure functionals (e.g. PBE[65]) because the computational scaling of hybrid functionals in periodic boxes or orders of magnitude worse than that of pure functionals. Therefore, it is of interest to compare the accuracy of predicted bulk properties of MLFFs that are trained to higher rungs of the "Jacob's ladder" of density functional approximations[66]. In the context of MLFFs for liquids, the current state of the art achieves DFT-level accuracy on prototypical systems like water[27, 45]. Moreover, most MLFFs that are developed for bulk property prediction are trained to a single chemical system, which lacks generalizability[27]. Recently, a HDNNP was developed for liquid water simulations and trained to hybrid DFT cluster data[45]. Overall, this model predicted accurate density and self-diffusivity[45]. In contrast, our model covers a broader chemical space, including common multi-component liquid electrolytes, and is validated more rigorously against multiple experimental of pure solvents and electrolyte mixtures.

Due to the superior quasi-linear scaling of the QRNN model[28] compared to the roughly cubic scaling of DFT, we are able run simulations on length and time scales that are impractical with pure DFT functionals**.** In addition, previous energy and force timing tests showed that the QRNN is ~10^4 faster compared to ωB97X-D/6-31G* on a single 2.4 GHz CPU[28]. With our current implementation we can achieve MD timings of ~200 ps/day on a GTX 1080 Ti GPU, affording physical simulation time of a few ns. However, due to memory limitations only ~1000 atoms can be simulated, which inhibits reliable transport property predictions of liquid electrolyte with high viscosities (> 3.0 cP). We anticipate that future work will be focused on the development of performant implementation of the QRNN model to facilitate simulations of longer time scales and larger systems.

Here, we also report some predicted properties which do not have yet experimental values available in the literature, such as the diffusivities of pure liquid solvents (i.e., VC, FEC, EMC and DEC). Although we cannot judge the accuracy of these predictions directly, our results for known properties suggest that they are reliable, and we hope to see them confirmed. The non-empirical nature of the method allows it to be used prospectively, to predict the transport properties of novel single- and multi-component electrolytes with quantitative accuracy—an exciting prospect for computational screening of materials. It also holds the promise of detailed structural analysis of transport properties such as Li ion diffusivity, which may be useful in structure-based design of electrolyte mixtures. Finally, the flexible functional form of HDNNPs should allow our model to be used in situations where atom type and covalent bond labels are not feasible, such as metals and redox reactions. Although not included in this work, this is a key motivation for the use of HDNNPs as we progress towards accurate atomistic simulations of battery materials to advance the development of the next generation of LIBs.

METHODS

Dataset construction: We have constructed a dataset for common electrolyte liquid simulations of common electrolytes using an active learning approach[41-44]. In summary, each active learning round (Scheme 1) is initialized by running MD of the systems in question (pure carbonates and/or mixed electrolytes). If a spurious reaction took place during MD, which is quite possible for HDNNPs, snapshots of the trajectory leading up to the reactive event were included. We found that including these reactive configurations helped the MD stability in the later rounds of active learning. Molecular clusters were extracted from the MD trajectories, then filtering of clusters based upon the uncertainty (ρ) of an ensemble of trained QRNN models, where $\rho = \frac{\sigma}{\sqrt{N_{atoms}}}$ and σ is the standard deviation of ensemble energy predictions. Here, any clusters that contained a value of 0.25 kcal mol^{-1} or lower were removed. After filtering, normal mode sampling (NMS)[32] was conducted to generate more geometry samples from the remaining clusters. This active learning loop was conducted for six cycles and is summarized in Scheme 1. The following sections

will describe the details of each round of active learning as it occurred any and additional sampling methods that were used.

The dataset was initialized by running MD of EC using the OPLS4[47] force field and extracting ~10K molecular clusters along the equilibrated trajectory. Random spherical clusters from MD simulations were extracted as follows. First, initial clusters from a given MD snapshot are created by iterating over each molecule—defining it as the central molecule—and extending the cluster if any atom of a neighboring molecule is within the radial cutoff of the atomic environment vector, which is 5.2 Å. These initial clusters are then filtered based upon the uniqueness of all the atomic pairwise distances. After filtering the initial clusters, random subclusters were selected up to a maximum size of five EC molecules. Pentamers were selected as the maximum cluster size since approximately five EC molecules would fit in a sphere with a radius of 5.2 Å, given the experimental density of EC at 313 K. It is important to note that the initial central molecule was not required to be in the subclusters, permitting sparse clusters to be generated. In addition, the number of clusters produced for a given cluster size (monomers up to pentamers) were weighted based upon the roughly cubic scaling of DFT ($N\_clusters \propto (\frac{1}{cluste\_size})^3$). After the clusters were extracted, the geometries of ~10% of the EC clusters were optimized using the previously reported SANI[67] model followed by NMS[32], to provide more samples near the equilibrium geometry of EC (which OPLS4 is not designed to reproduce, particularly as regards exact bond lengths). These initial 119,381 datapoints were labeled with the reference level of theory. From this dataset, a five-member ensemble was trained, with each member being initialized with a different random seed.

For the first three rounds of active learning, the dataset was composed only of clusters of pure EC, with no other chemical species. In round two, EC cluster datapoints were generated from pure EC MD at conditions 313 K / 1 atm, 423 K / 1 atm, and313 K / 10 atm. In round four, DMC, PC, Li^+, and PF_6^- were introduced. For DMC and PC, round four sampling was performed using liquid MD at 298 K with the round 3 model, followed by cluster extraction, filtering, and NMS. For Li^+ and PF_6^-, ions were inserted into a ~1% subset of the EC clusters that were generated in the first three rounds. The ions were inserted

into each cluster of EC molecules at random position and orientation, then filtered by checking if any ion atom was closer than 1.0 Å or further than 4.0 Å from any of the EC atoms. The atomic positions of these new datapoints with Li^+ and PF_6^- were then optimized using GFN2xTB[68] with a loose convergence criterion of 10 kcal/mol/Å. This allowed reasonable geometries for the ion-containing clusters without having to rely on OPLS4, which was expected to be less reliable for these geometries.

For rounds five and six, a periodic system with ~200 randomly placed molecules, with an equal number of the seven common carbonates listed above and $LiPF_6$, was used for MD sampling. This system allowed us to collect diverse cluster datapoints of mixed carbonates with $LiPF_6$. Lastly, we sampled the decomposition of monomers of the seven common carbonates, and dimers that included the seven common carbonates plus either Li^+ or PF_6^- . This decomposition sampling added 1193 new datapoints, mostly high-energy geometries, which further helped the MD stability when using the QRNN potential by instructing the QRNN model that these were unfavorable. The decomposition sampling began by scaling all intermolecular distance by +/- 20% (of course, the monomers had no intermolecular degrees of freedom). After the scaling the intermolecular distance, the internal degrees of freedom were randomly perturbed according to a normal distribution (+/- representing the standard deviation): bonds (+/- 0.1 Å), angles (+/- 15°), torsions (+/- 20°), and Cartesian coordinates (+/- 0.1 Å). This was followed by stretching each bond individually, in steps of 10%: 1.0x, 1.1x, 1.21x, 1.33, 1.45, and 1.61x its original length.

During the round 6 MD simulations of mixed carbonate systems with high salt concentrations we observed the formation of unphysical Li^+ ion clusters. These unphysical clusters contained up to four Li^+ ions with the Li^+-Li^+ closest distance being < 3.0 Å. Furthermore, once formed, the Li^+ ion clusters did not dissociate within the simulation time of 1 ns. In our last round of active learning (round 7) our sampling strategy was focused on fixing this Li^+ ion clustering problem. Therefore, we extracted clusters from round 6 MD and removed any cluster that did not have at least 2 Li^+ ions. In addition, we added cluster datapoints extracted from MD simulations of racemic mixtures of FEC and PC. These cluster datapoints

were then used as input to the empirical sampling protocol described above, resulting in 54,498 new datapoints.

In total, 362,382 datapoints were generated from the seven rounds of active learning. DFT energies, atomic forces, and dipoles were calculated for each datapoint. All DFT calculations were conducted using the ωB97X-D3BJ[69, 70] functional and the def2-TZVPD[71] basis set with the electronic structure software package Psi4-1.3[72]. Each single-point energy calculation was performed using density fitting, a 1e-10 DFT basis tolerance, a 1e-10 Schwarz screening threshold, and a 1e-6 linear dependency cutoff.

Model training: As stated above, we used the previously reported QRNN architecture[28] to train our electrolyte models using a locally modified copy of torchani open source software package[25, 73]. Some small differences in the training protocol were used compared to the training of the direct learned ionic QRNN model previously reported[28]. Specifically, throughout the active learning process we trained to both energy and dipoles labels via multitask learning[74, 75] while using early stopping and a 1% learning rate decay on plateau, with a patience of zero and a maximum of 500 epochs. In our last three models we included the force error in the multitask loss function during the training. For the training of our final model, we pruned the dataset by filtering any datapoints where the force on any atom > 0.5 Hartree/Å. After force filtering, the dataset was further pruned by removing any datapoints where the energy (after removing linear atomic energies) was greater than 10x the standard deviation from the mean of each net charge state. This resulted in 40,252 datapoints that were removed. Lastly, weight normalization[76] was used during the training of our last mode. With the initialization described by Arpit and co-workers[77] except that g was capped at 2.0. The norms of the weight matrix columns, g, were subsequently excluded from the optimization. We found that this change reduced the dependence on weight decay regularization and produced more stable MD.

Molecular dynamics: All the molecular dynamics (MD) simulations of liquid electrolytes were performed using the QRNN force field implemented as a calculator in the Atomic Simulation Environment (ASE) package[78] using a constant time step of 0.5 fs. All simulations were performed using NPT or NVT

ensembles, as appropriate, with the Nose-Hoover thermostat and Parrinello-Rahman (PR) barostat[79]. A relaxation time constant of 0.05 ps was chosen for the thermostat and 2.5 ps for the barostat. The initial geometries of the liquid electrolytes were created using Disordered System Builder as implemented in Maestro. The total number of atoms in each system was limited to ~1000 atoms to maintain a balance between the computational cost of the MD simulations and the GPU memory. The initial dimensions of the cubic boxes were determined using the experimental densities of the pure solvents. For the systems containing $LiPF_6$ salt, the number of molecules of the $LiPF_6$ salt were calculated based on the volume of the initial box created for the corresponding pure solvent system and the salt concentration. A summary of the number of molecules of the solvent, $LiPF_6$ salt and the dimensions of the initial simulation boxes are provided in Table S1. We performed additional benchmarking simulations for each liquid electrolyte systems using the OPLS4[47] force field as implemented in the MD package Desmond[80]. The initial geometries for the OPLS4[47] systems were created with 8 times the number of molecules and 8 times the volume of the initial simulation box of the corresponding QRNN system, allowing to reduce time and box size convergence effects. Additional details regarding thermodynamic and transport property predictions can be found the supporting information.

TABLES AND FIGURES

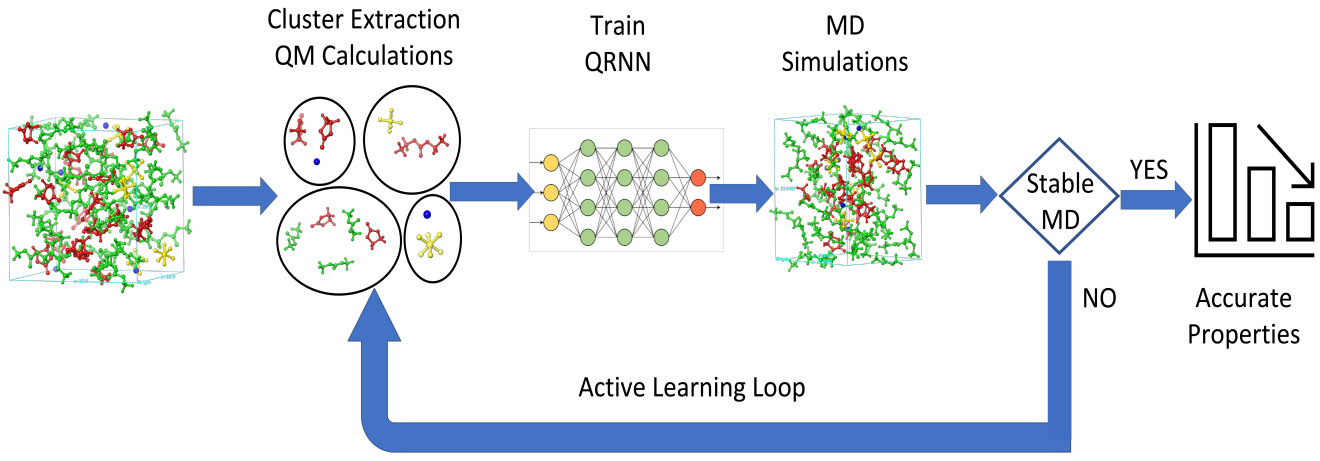

Scheme 1: Overview of the active learning process utilized to construct the QRNN potential for liquid electrolyte simulations. The cycle is initialized by running MD, followed by extracting clusters. The cluster training data is labeled with the ωB97X-D3BJ/def2-TZVPD reference level of theory. Once the new data is added to the dataset an ensemble of QRNN models is trained, followed by MD. This cycle was repeated for six rounds, which resulted in a stable potential for pure carbonate and mixed electrolyte liquid simulations.

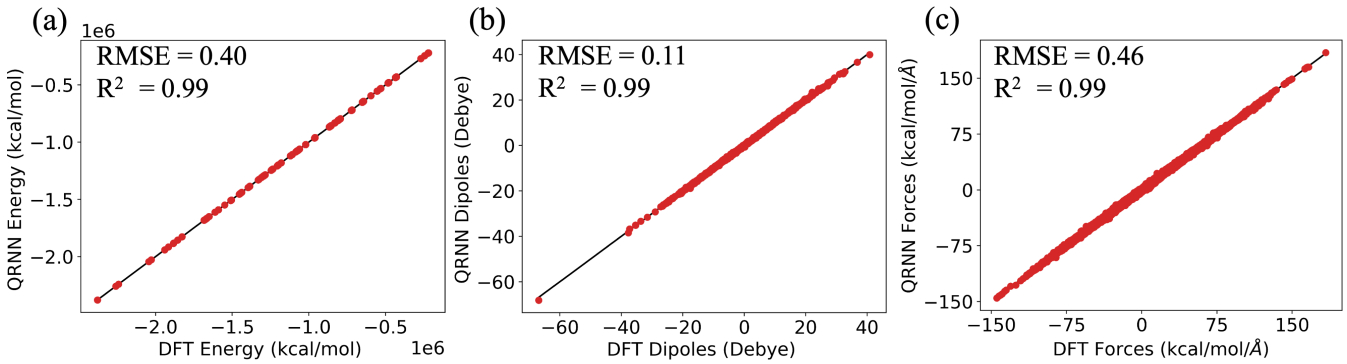

Figure 1: Correlation of ωB97X-D3BJ/def2-TZVPD cluster test set energies (left), dipole x, y, z components (center), and atomic force x, y, z components (right) to the QRNN predictions.

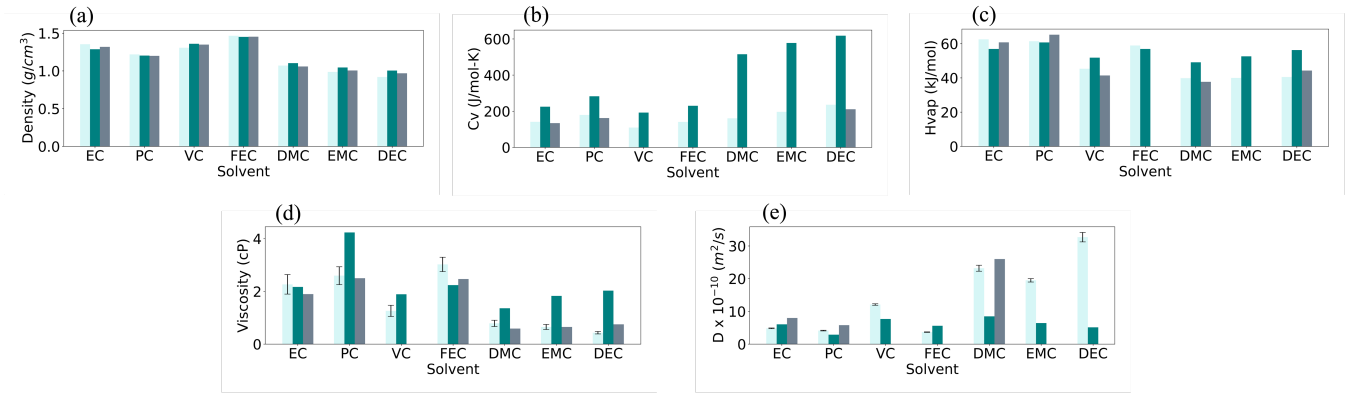

Figure 2: Comparison of the QRNN and OPLS4 computed and experimental values of (a) density[51, 54, 56], (b) specific heat at constant volume (C_v)[49, 50], (c) heat of vaporization (H_{vap})[21, 48, 52, 53, 55], (d) self-diffusivity[59] and (e) viscosity[54, 56, 58] for pure liquid carbonate solvents. The error bars for the QRNN self-diffusivity and viscosity values are obtained by bootstrapping.

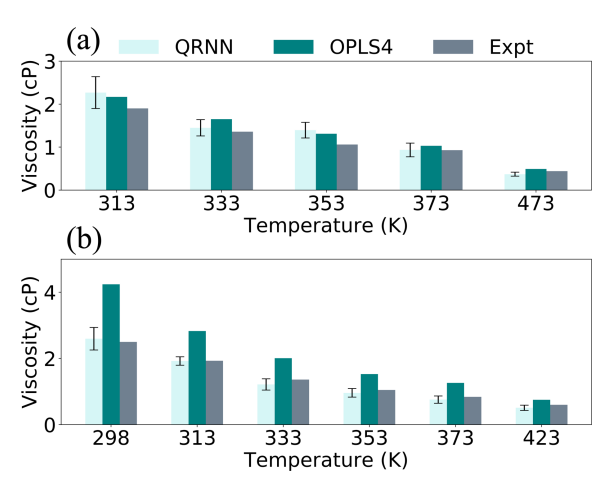

Figure 3: Temperature dependence of the viscosities of liquid (a) EC and (b) PC computed using QRNN, OPLS4 and compared with experimental data[60].

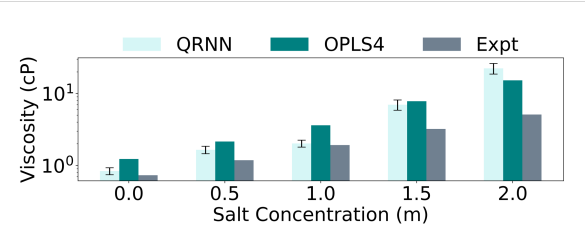

Figure 4: Figure 4: Viscosity as a function of LiPF6 salt concentration for EC:DMC (3:7) with 0-2 m LiPF6 salt computed using QRNN, OPLS4 and compared with experimental data[61].

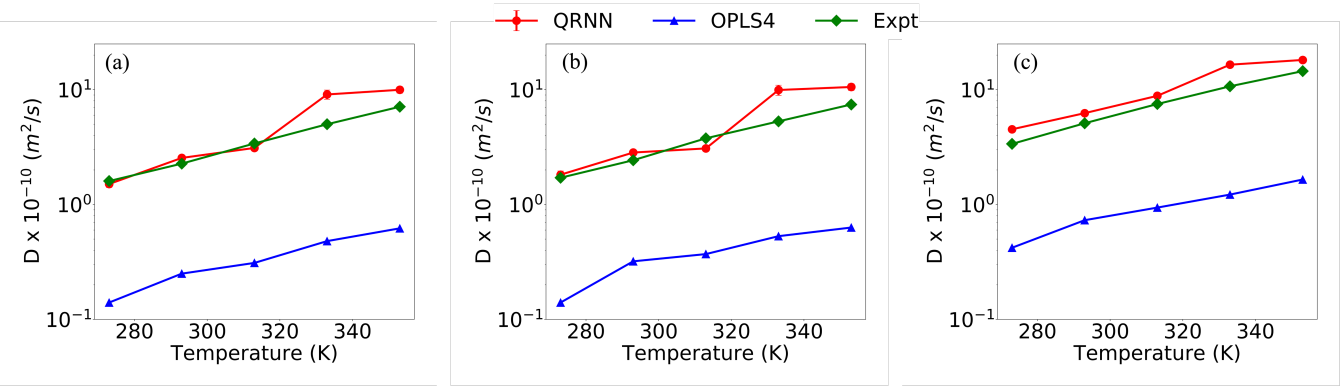

Figure 5: Temperature dependence of diffusivity[62] of (a) Li^+, (b) PF_6^- and (c) DEC for DEC + 1M $LiPF_6$ electrolyte.

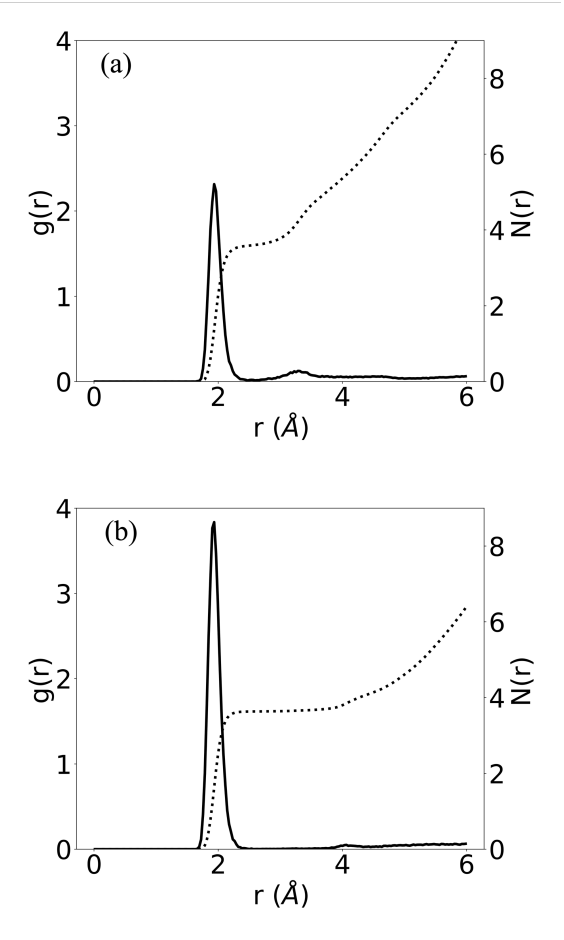

Figure 6: The Li^+-Oc radial distribution function (solid line) and the running coordination number (dished line) from QRNN MD simulations of EC + 1 M $LiPF_6$ (a) and DMC + 1 M $LiPF_6$ (b).

ASSOCIATED CONTENT

Supporting Information

Simulation details for computing thermodynamic and transport properties, MD stability analysis, Li ion solvation structure analysis, and additional tables and figures showing model results and comparisons to OPLS4 and experimental data (PDF). The training dataset in JSON format with reference labels.

Corresponding Authors

Steven Dajnowicz - Schrödinger, Inc., New York, New York 10036, United States; Email: steven.dajnowicz@schrodinger.com

Garvit Agarwal - Schrödinger, Inc., New York, New York 10036, United States; Email: garvit.agarwal@schrodinger.com

Funding Sources

This work is supported and funded by the Bill and Melinda Gates Foundation.

Author Contributions

‡ These authors contributed equally to this work

Notes

The authors declare no competing financial interest

ACKNOWLEDGMENT

We would like to thank Nongnuch Artrith, Alexander Urban, and the other members of the Columbia Center for Computational Electrochemistry for useful discussions.

REFERENCE

1. Goodenough, J. B.; Park, K.-S., The Li-ion rechargeable battery: a perspective. *Journal of the American Chemical Society* **2013,** *135* (4), 1167-1176.
2. Tarascon, J.-M.; Armand, M., Issues and challenges facing rechargeable lithium batteries. *Nature* **2011**, 171-179.
3. Bruce, P. G., Energy storage beyond the horizon: Rechargeable lithium batteries. *Solid State Ionics* **2008,** *179* (21-26), 752-760.
4. Goodenough, J. B.; Kim, Y., Challenges for rechargeable Li batteries. *Chemistry of materials* **2010,** *22* (3), 587-603.
5. Urban, A.; Seo, D.-H.; Ceder, G., Computational understanding of Li-ion batteries. *npj Computational Materials* **2016,** *2* (1), 1-13.
6. Curtarolo, S.; Hart, G. L.; Nardelli, M. B.; Mingo, N.; Sanvito, S.; Levy, O., The high-throughput highway to computational materials design. *Nature materials* **2013,** *12* (3), 191-201.
7. Wang, A.; Kadam, S.; Li, H.; Shi, S.; Qi, Y., Review on modeling of the anode solid electrolyte interphase (SEI) for lithium-ion batteries. *npj Computational Materials* **2018,** *4* (1), 1-26.
8. Hohenberg, P.; Kohn, W., Inhomogeneous electron gas. *Physical review* **1964,** *136* (3B), B864.
9. Kohn, W.; Sham, L. J., Self-consistent equations including exchange and correlation effects. *Physical review* **1965,** *140* (4A), A1133.
10. Leung, K., Two-electron reduction of ethylene carbonate: A quantum chemistry re-examination of mechanisms. *Chemical Physics Letters* **2013,** *568*, 1-8.

11. Leung, K.; Budzien, J. L., Ab initio molecular dynamics simulations of the initial stages of solid–electrolyte interphase formation on lithium ion battery graphitic anodes. *Physical Chemistry Chemical Physics* **2010,** *12* (25), 6583-6586.
12. Yu, J.; Balbuena, P. B.; Budzien, J.; Leung, K., Hybrid DFT functional-based static and molecular dynamics studies of excess electron in liquid ethylene carbonate. *Journal of The Electrochemical Society* **2011,** *158* (4), A400.
13. de la Hoz, J. M. M.; Balbuena, P. B., Reduction mechanisms of additives on Si anodes of Li-ion batteries. *Physical Chemistry Chemical Physics* **2014,** *16* (32), 17091-17098.
14. Leung, K.; Rempe, S. B.; Foster, M. E.; Ma, Y.; del la Hoz, J. M. M.; Sai, N.; Balbuena, P. B., Modeling electrochemical decomposition of fluoroethylene carbonate on silicon anode surfaces in lithium ion batteries. *Journal of the Electrochemical Society* **2013,** *161* (3), A213.
15. Wang, Y.; Balbuena, P. B., Theoretical insights into the reductive decompositions of propylene carbonate and vinylene carbonate: density functional theory studies. *The Journal of Physical Chemistry B* **2002,** *106* (17), 4486-4495.
16. Wang, Y.; Nakamura, S.; Tasaki, K.; Balbuena, P. B., Theoretical studies to understand surface chemistry on carbon anodes for lithium-ion batteries: how does vinylene carbonate play its role as an electrolyte additive? *Journal of the American Chemical Society* **2002,** *124* (16), 4408-4421.
17. Wang, Y.; Nakamura, S.; Ue, M.; Balbuena, P. B., Theoretical studies to understand surface chemistry on carbon anodes for lithium-ion batteries: reduction mechanisms of ethylene carbonate. *Journal of the American Chemical Society* **2001,** *123* (47), 11708-11718.
18. Winter, M., The solid electrolyte interphase–the most important and the least understood solid electrolyte in rechargeable Li batteries. *Zeitschrift für physikalische Chemie* **2009,** *223* (10-11), 1395-1406.
19. Harrison, J. A.; Schall, J. D.; Maskey, S.; Mikulski, P. T.; Knippenberg, M. T.; Morrow, B. H., Review of force fields and intermolecular potentials used in atomistic computational materials research. *Applied Physics Reviews* **2018,** *5* (3), 031104.
20. Borodin, O.; Smith, G. D., Quantum chemistry and molecular dynamics simulation study of dimethyl carbonate: ethylene carbonate electrolytes doped with LiPF6. *The Journal of Physical Chemistry B* **2009,** *113* (6), 1763-1776.
21. Silva, L. B.; Freitas, L. C. G., Structural and thermodynamic properties of liquid ethylene carbonate and propylene carbonate by Monte Carlo Simulations. *Journal of Molecular Structure: THEOCHEM* **2007,** *806* (1-3), 23-34.
22. von Wald Cresce, A.; Borodin, O.; Xu, K., Correlating Li+ solvation sheath structure with interphasial chemistry on graphite. *The Journal of Physical Chemistry C* **2012,** *116* (50), 26111-26117.
23. Islam, M. M.; Kolesov, G.; Verstraelen, T.; Kaxiras, E.; Van Duin, A. C., eReaxFF: a pseudoclassical treatment of explicit electrons within reactive force field simulations. *Journal of chemical theory and computation* **2016,** *12* (8), 3463-3472.
24. Islam, M. M.; Van Duin, A. C., Reductive decomposition reactions of ethylene carbonate by explicit electron transfer from lithium: an eReaxFF molecular dynamics study. *The Journal of Physical Chemistry C* **2016,** *120* (48), 27128-27134.
25. Kim, S.-P.; Van Duin, A. C.; Shenoy, V. B., Effect of electrolytes on the structure and evolution of the solid electrolyte interphase (SEI) in Li-ion batteries: A molecular dynamics study. *Journal of Power Sources* **2011,** *196* (20), 8590-8597.
26. Van Duin, A. C.; Dasgupta, S.; Lorant, F.; Goddard, W. A., ReaxFF: a reactive force field for hydrocarbons. *The Journal of Physical Chemistry A* **2001,** *105* (41), 9396-9409.
27. Behler, J. r., Four generations of high-dimensional neural network potentials. *Chemical Reviews* **2021**.
28. Jacobson, L. D.; Stevenson, J. M.; Ramezanghorbani, F.; Ghoreishi, D.; Leswing, K.; Harder, E. D.; Abel, R., Transferable Neural Network Potential Energy Surfaces for Closed-Shell Organic Molecules: Extension to Ions. *Journal of Chemical Theory and Computation* **2022**.

29. Ko, T. W.; Finkler, J. A.; Goedecker, S.; Behler, J., A fourth-generation high-dimensional neural network potential with accurate electrostatics including non-local charge transfer. *Nature communications* **2021,** *12* (1), 1-11.
30. Qiao, Z.; Welborn, M.; Anandkumar, A.; Manby, F. R.; Miller III, T. F., OrbNet: Deep learning for quantum chemistry using symmetry-adapted atomic-orbital features. *The Journal of Chemical Physics* **2020,** *153* (12), 124111.
31. Schütt, K. T.; Sauceda, H. E.; Kindermans, P.-J.; Tkatchenko, A.; Müller, K.-R., Schnet–a deep learning architecture for molecules and materials. *The Journal of Chemical Physics* **2018,** *148* (24), 241722.
32. Smith, J. S.; Isayev, O.; Roitberg, A. E., ANI-1: an extensible neural network potential with DFT accuracy at force field computational cost. *Chemical science* **2017,** *8* (4), 3192-3203.
33. Smith, J. S.; Nebgen, B. T.; Zubatyuk, R.; Lubbers, N.; Devereux, C.; Barros, K.; Tretiak, S.; Isayev, O.; Roitberg, A. E., Approaching coupled cluster accuracy with a general-purpose neural network potential through transfer learning. *Nature communications* **2019,** *10* (1), 1-8.
34. Unke, O. T.; Meuwly, M., PhysNet: a neural network for predicting energies, forces, dipole moments, and partial charges. *Journal of chemical theory and computation* **2019,** *15* (6), 3678-3693.
35. Deringer, V. L., Modelling and understanding battery materials with machine-learning-driven atomistic simulations. *Journal of Physics: Energy* **2020,** *2* (4), 041003.
36. Shao, Y.; Knijff, L.; Dietrich, F. M.; Hermansson, K.; Zhang, C., Modelling bulk electrolytes and electrolyte interfaces with atomistic machine learning. *Batteries & Supercaps* **2021,** *4* (4), 585-595.
37. Artrith, N., Machine learning for the modeling of interfaces in energy storage and conversion materials. *Journal of Physics: Energy* **2019,** *1* (3), 032002.
38. Artrith, N.; Urban, A.; Ceder, G., Constructing first-principles phase diagrams of amorphous Li x Si using machine-learning-assisted sampling with an evolutionary algorithm. *The Journal of chemical physics* **2018,** *148* (24), 241711.
39. Deringer, V. L.; Merlet, C.; Hu, Y.; Lee, T. H.; Kattirtzi, J. A.; Pecher, O.; Csányi, G.; Elliott, S. R.; Grey, C. P., Towards an atomistic understanding of disordered carbon electrode materials. *Chemical communications* **2018,** *54* (47), 5988-5991.
40. Li, W.; Ando, Y.; Minamitani, E.; Watanabe, S., Study of Li atom diffusion in amorphous Li3PO4 with neural network potential. *The Journal of chemical physics* **2017,** *147* (21), 214106.
41. Artrith, N.; Behler, J., High-dimensional neural network potentials for metal surfaces: A prototype study for copper. *Physical Review B* **2012,** *85* (4), 045439.
42. Podryabinkin, E. V.; Shapeev, A. V., Active learning of linearly parametrized interatomic potentials. *Computational Materials Science* **2017,** *140*, 171-180.
43. Smith, J. S.; Nebgen, B.; Lubbers, N.; Isayev, O.; Roitberg, A. E., Less is more: Sampling chemical space with active learning. *The Journal of chemical physics* **2018,** *148* (24), 241733.
44. Zhang, L.; Lin, D.-Y.; Wang, H.; Car, R.; Weinan, E., Active learning of uniformly accurate interatomic potentials for materials simulation. *Physical Review Materials* **2019,** *3* (2), 023804.
45. Zaverkin, V.; Holzmüller, D.; Schuldt, R.; Kästner, J., Predicting properties of periodic systems from cluster data: A case study of liquid water. *The Journal of Chemical Physics* **2022,** *156* (11), 114103.
46. Smith, J. S.; Zubatyuk, R.; Nebgen, B.; Lubbers, N.; Barros, K.; Roitberg, A. E.; Isayev, O.; Tretiak, S., The ANI-1ccx and ANI-1x data sets, coupled-cluster and density functional theory properties for molecules. *Scientific data* **2020,** *7* (1), 1-10.
47. Lu, C.; Wu, C.; Ghoreishi, D.; Chen, W.; Wang, L.; Damm, W.; Ross, G. A.; Dahlgren, M. K.; Russell, E.; Von Bargen, C. D., OPLS4: Improving Force Field Accuracy on Challenging Regimes of Chemical Space. *Journal of Chemical Theory and Computation* **2021**.
48. Choi, J. K.; Joncich, M. J., Heats of combustion, heats of formation, and vapor pressures of some organic carbonates. Estimation of carbonate group contribution to heat of formation. *Journal of Chemical & Engineering Data* **1971,** *16* (1), 87-90.

49. Kolosovskii, N. A. U., W.W., Specific heat of liquids. II. *Zhur. Obshchei Khim* **1934**, 1027-1033.
50. Peppel, W., Preparation and properties of the alkylene carbonates. *Industrial & Engineering Chemistry* **1958,** *50* (5), 767-770.
51. Sasaki, Y., Physical and electrochemical properties and application to lithium batteries of fluorinated organic solvents. In *Fluorinated Materials for Energy Conversion*, Elsevier: 2005; pp 285-304.
52. Steele, W.; Chirico, R.; Knipmeyer, S.; Nguyen, A.; Smith, N., Thermodynamic properties and ideal-gas enthalpies of formation for dicyclohexyl sulfide, diethylenetriamine, di-n-octyl sulfide, dimethyl carbonate, piperazine, hexachloroprop-1-ene, tetrakis (dimethylamino) ethylene, N, N '-bis-(2-hydroxyethyl) ethylenediamine, and 1, 2, 4-triazolo [1, 5-a] pyrimidine. *Journal of Chemical & Engineering Data* **1997,** *42* (6), 1037-1052.
53. Stull, D. R., Vapor Pressure of Pure Substances. Organic and Inorganic Compounds. *Ind. Eng. Chem* **1947,** *39* (4), 517-540.
54. Väli, R.; Jänes, A.; Lust, E., Vinylene carbonate as co-solvent for low-temperature mixed electrolyte based Supercapacitors. *Journal of The Electrochemical Society* **2016,** *163* (6), A851.
55. Verevkin, S. P.; Toktonov, A. V.; Chernyak, Y.; Schäffner, B.; Börner, A., Vapour pressure and enthalpy of vaporization of cyclic alkylene carbonates. *Fluid phase equilibria* **2008,** *268* (1-2), 1-6.
56. Xu, K., Nonaqueous liquid electrolytes for lithium-based rechargeable batteries. *Chemical reviews* **2004,** *104* (10), 4303-4418.
57. Maginn, E. J.; Messerly, R. A.; Carlson, D. J.; Roe, D. R.; Elliot, J. R., Best practices for computing transport properties 1. Self-diffusivity and viscosity from equilibrium molecular dynamics [article v1. 0]. *Living Journal of Computational Molecular Science* **2019,** *1* (1), 6324-6324.
58. Jänes, A.; Thomberg, T.; Eskusson, J.; Lust, E., Fluoroethylene Carbonate and Propylene Carbonate Mixtures Based Electrolytes for Supercapacitors. *ECS Transactions* **2014,** *58* (27), 71.
59. Hayamizu, K.; Aihara, Y.; Arai, S.; Martinez, C. G., Pulse-gradient spin-echo 1H, 7Li, and 19F NMR diffusion and ionic conductivity measurements of 14 organic electrolytes containing LiN (SO2CF3) 2. *The Journal of Physical Chemistry B* **1999,** *103* (3), 519-524.
60. Flick, E. W., *Industrial solvents handbook*. 5th ed.; William Andrew Publishing: 1998.
61. Logan, E.; Tonita, E. M.; Gering, K.; Li, J.; Ma, X.; Beaulieu, L.; Dahn, J., A study of the physical properties of Li-ion battery electrolytes containing esters. *Journal of The Electrochemical Society* **2018,** *165* (2), A21.
62. Hayamizu, K., Temperature dependence of self-diffusion coefficients of ions and solvents in ethylene carbonate, propylene carbonate, and diethyl carbonate single solutions and ethylene carbonate+ diethyl carbonate binary solutions of LiPF6 studied by NMR. *Journal of Chemical & Engineering Data* **2012,** *57* (7), 2012-2017.
63. Ganesh, P.; Jiang, D.-e.; Kent, P., Accurate static and dynamic properties of liquid electrolytes for Li-ion batteries from ab initio molecular dynamics. *The Journal of Physical Chemistry B* **2011,** *115* (12), 3085-3090.
64. Chaudhari, M. I.; Nair, J. R.; Pratt, L. R.; Soto, F. A.; Balbuena, P. B.; Rempe, S. B., Scaling atomic partial charges of carbonate solvents for lithium ion solvation and diffusion. *Journal of chemical theory and computation* **2016,** *12* (12), 5709-5718.
65. Perdew, J. P.; Burke, K.; Ernzerhof, M., Generalized gradient approximation made simple (vol 77, pg 3865, 1996). AMERICAN PHYSICAL SOC ONE PHYSICS ELLIPSE, COLLEGE PK, MD 20740-3844 USA: 1997; Vol. 78, pp 1396-1396.
66. Perdew, J. P.; Schmidt, K. In *Jacob's ladder of density functional approximations for the exchange-correlation energy*, AIP Conference Proceedings, American Institute of Physics: 2001; pp 1-20.
67. Stevenson, J. M.; Jacobson, L. D.; Zhao, Y.; Wu, C.; Maple, J.; Leswing, K.; Harder, E.; Abel, R., Schr\" odinger-ANI: An Eight-Element Neural Network Interaction Potential with Greatly Expanded Coverage of Druglike Chemical Space. *arXiv preprint arXiv:1912.05079* **2019**.

68. Bannwarth, C.; Ehlert, S.; Grimme, S., GFN2-xTB—An accurate and broadly parametrized self-consistent tight-binding quantum chemical method with multipole electrostatics and density-dependent dispersion contributions. *Journal of chemical theory and computation* **2019,** *15* (3), 1652-1671.
69. Grimme, S.; Ehrlich, S.; Goerigk, L., Effect of the damping function in dispersion corrected density functional theory. *Journal of computational chemistry* **2011,** *32* (7), 1456-1465.
70. Mardirossian, N.; Head-Gordon, M., ωB97X-V: A 10-parameter, range-separated hybrid, generalized gradient approximation density functional with nonlocal correlation, designed by a survival-of-the-fittest strategy. *Physical Chemistry Chemical Physics* **2014,** *16* (21), 9904-9924.
71. Weigend, F., Accurate Coulomb-fitting basis sets for H to Rn. *Physical chemistry chemical physics* **2006,** *8* (9), 1057-1065.
72. Turney, J. M.; Simmonett, A. C.; Parrish, R. M.; Hohenstein, E. G.; Evangelista, F. A.; Fermann, J. T.; Mintz, B. J.; Burns, L. A.; Wilke, J. J.; Abrams, M. L., Psi4: an open-source ab initio electronic structure program. *Wiley Interdisciplinary Reviews: Computational Molecular Science* **2012,** *2* (4), 556-565.
73. Gao, X.; Ramezanghorbani, F.; Isayev, O.; Smith, J. S.; Roitberg, A. E., TorchANI: a free and open source PyTorch-based deep learning implementation of the ANI neural network potentials. *Journal of chemical information and modeling* **2020,** *60* (7), 3408-3415.
74. Kendall, A.; Gal, Y.; Cipolla, R. In *Multi-task learning using uncertainty to weigh losses for scene geometry and semantics*, Proceedings of the IEEE conference on computer vision and pattern recognition, 2018; pp 7482-7491.
75. Ramezanghorbani, F. Developing Machine Learning Models to Enhance Applicability of Neural Network Potentials in Drug Discovery. University of Florida, 2020.
76. Salimans, T.; Kingma, D. P., Weight normalization: A simple reparameterization to accelerate training of deep neural networks. *Advances in neural information processing systems* **2016,** *29*.
77. Arpit, D.; Campos, V.; Bengio, Y., How to initialize your network? robust initialization for weightnorm & resnets. *Advances in Neural Information Processing Systems* **2019,** *32*.
78. Larsen, A. H.; Mortensen, J. J.; Blomqvist, J.; Castelli, I. E.; Christensen, R.; Dułak, M.; Friis, J.; Groves, M. N.; Hammer, B.; Hargus, C., The atomic simulation environment—a Python library for working with atoms. *Journal of Physics: Condensed Matter* **2017,** *29* (27), 273002.
79. Melchionna, S., Constrained systems and statistical distribution. *Physical Review E* **2000,** *61* (6), 6165.
80. Bowers, K. J.; Chow, D. E.; Xu, H.; Dror, R. O.; Eastwood, M. P.; Gregersen, B. A.; Klepeis, J. L.; Kolossvary, I.; Moraes, M. A.; Sacerdoti, F. D. In *Scalable algorithms for molecular dynamics simulations on commodity clusters*, SC'06: Proceedings of the 2006 ACM/IEEE Conference on Supercomputing, IEEE: 2006; pp 43-43.